Functional integrity and stable high-temperature operation of planarized ultraviolet-A $Al_xGa_{1-x}N/Al_yGa_{1-y}N$ multiple-quantum-disk nanowire LEDs with charge-conduction promoting interlayer

Abdullah A. Alhamoud[a,b,†], Nasir Alfaraj[a,†], Davide Priante[a], Bilal Janjua[a], Abdullah A. Alatawi[a,b], Abdulrahman M. Albadri[b], Ahmed Y. Alyamani[b], Tien Khee Ng[a], and Boon S. Ooi[a,*]

[a]Photonics Laboratory, King Abdullah University of Science and Technology (KAUST), Thuwal 23955-6900, Kingdom of Saudi Arabia
[b]National Center for Nanotechnology, King Abdulaziz City for Science and Technology (KACST), Riyadh 11442-6086, Kingdom of Saudi Arabia

ABSTRACT

Unprecedented high-temperature operational stability of interfacial silicide-free ultraviolet-A multiple-quantum-disk AlGaN nanowire-based light-emitting diodes on metal is achieved and investigated. Reasonable variations in device operational parameters across a wide range of temperatures demonstrate the high quality of the layer interfaces and efficient carrier injection. We previously presented ultraviolet-A quantum-confined $Al_xGa_{1-x}N/Al_yGa_{1-y}N$ nanowire-based light-emitting diodes and studied their steady-state electro- and photoluminescent characteristics at room temperature [Priante et al., Opt. Mater. Express 7(12), 4214 (2017)]. Herein, we significantly expand the scope of our previous work by investigating the operational stability of the device across a wide range of temperatures (−50–100 °C) with conformal parylene-C deposition, forming a nanowire forest as a polymer/nanowire three-dimensional composite material. This work constitutes part of a larger study into the operational stability of ultraviolet light-emitting diode chemical sensors at a wide range of temperatures for operation in harsh environments such as in downhole oil exploration.

Keywords: Ultraviolet-A, $Al_xGa_{1-x}N$, nanowire-based LEDs, QDisks, high-temperature operation, stability, downhole sensing.

1. INTRODUCTION

In recent years, the heterogeneous integration of a variety of inorganic materials for fabricating electronic and optoelectronic devices on sapphire[1,2] and silicon (Si)[3–8] has shown clear promise in reshaping the future of the electronics industry. Additionally, the high thermal and chemical stability of the group III–nitride material system indicates its potential application in harsh environments in comparison to conventional silicon-based optoelectronic devices, which have limited operating temperature range and require extra protective packaging.[9,10] Ultraviolet (UV)-emitting group III–nitride materials show promising potential for a variety of multifunctional applications, including solid-state lighting technology,[11] water purification,[12] and possibly downhole photosensing.[13] With the wide range of wavelength tunability available to these materials, the most promising germicidal UV devices are based on aluminum gallium nitride and its alloys ($Al_xGa_{1-x}N$, where $0 < x \leq 1$), and one of the most critical applications of $Al_xGa_{1-x}N$-based nanowire devices is water sterilization, particularly in highly water-stressed countries.[14] Moreover, the field of downhole photonics has progressed steadily since it emerged in the late 1980s, and UV sensors, combined with optical density measurements, are crucial for the classification of oil samples. Methods for discriminating between oil samples are dependent on the optical absorption spectrum

[†]A. Alhamoud and N. Alfaraj contributed equally to this work.
[*]Further author information: (Send correspondence to Prof. Boon S. Ooi).
[*]E-mail: boon.ooi@kaust.edu.sa; telephone: +966 (54) 470–0036.

Gallium Nitride Materials and Devices XIV, edited by Hiroshi Fujioka, Hadis Morkoç, Ulrich T. Schwarz, Proc. of SPIE Vol. 10918, 109181X · © 2019 SPIE
CCC code: 0277-786X/19/$18 · doi: 10.1117/12.2506210

of all crude oils in the visible and near-infrared range (and in the ultraviolet range when desired),[15] which can be discerned through optical density measurements using[13]

$$\mathrm{OD} = Ce^{\gamma E_\nu}, \tag{1}$$

where OD is the optical density, C is a crude oil identification constant, γ is an exponential decay value (in cm), which is fairly constant for different spectra, and E_ν is the photon energy in wavenumbers (cm^{-1}). Such applications require highly stable UV devices suitable for use in high-temperature and otherwise harsh environments.[13,16,17] We have previously grown and fabricated UV-A quantum-confined $\mathrm{Al}_x\mathrm{Ga}_{1-x}\mathrm{N}/\mathrm{Al}_y\mathrm{Ga}_{1-y}\mathrm{N}$ nanowire-based light-emitting diodes (LEDs) and examined their steady-state electro- and photoluminescent characteristics at room temperature.[18,19] Here, we expand the scope of that work by investigating the operational stability of the device across a wide range of operation temperatures (T), namely −50–100 °C, electromechanically supported by a conformal parylene-C planarization layer, forming a nanowire forest as a polymer/nanowire three-dimensional (3D) composite material.

2. NANOWIRE GROWTH AND DEVICE FABRICATION

Figure 1(a) shows the schematic structure of the UV-A quantum-confined $\mathrm{Al}_x\mathrm{Ga}_{1-x}\mathrm{N}/\mathrm{Al}_y\mathrm{Ga}_{1-y}\mathrm{N}$ nanowires. The scanning electron microscopy (SEM) images in Figure 1(b) demonstrate that the nanowires were highly uniform and aligned along the vertical c-axis, while the transmission electron microscopy (TEM) image in Figure 1(c) shows a high-resolution cross-sectional image of an ensemble of the epitaxially grown nanowires.

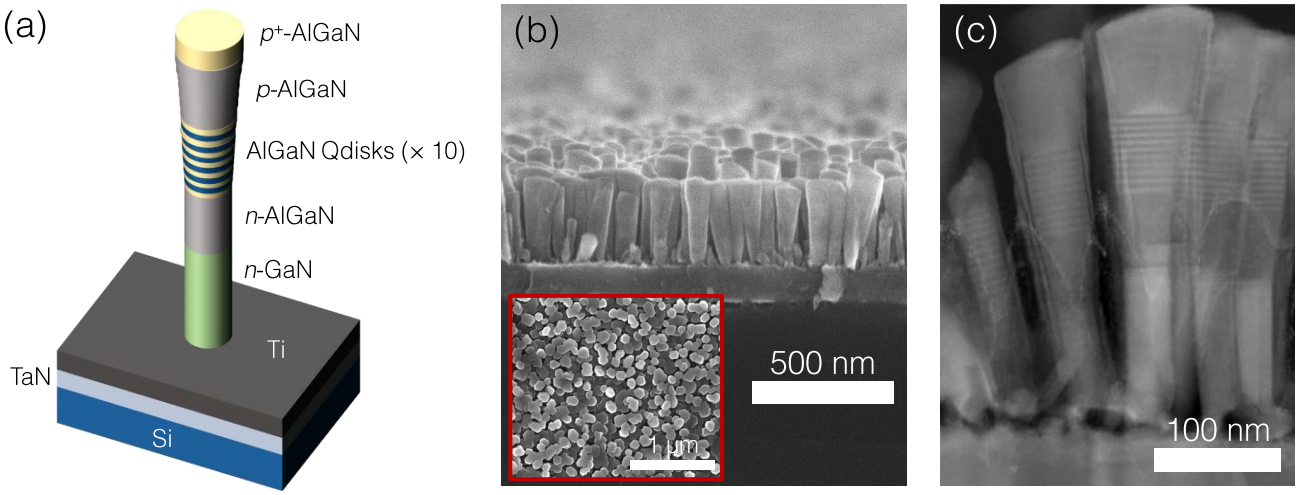

Figure 1. (a) The schematic structure of the UV-A quantum-confined $\mathrm{Al}_x\mathrm{Ga}_{1-x}\mathrm{N}$ (3 nm)/$\mathrm{Al}_y\mathrm{Ga}_{1-y}\mathrm{N}$ (4 nm) nanowires, with the growth direction normal to the substrate along the c-axis. (b) A cross-sectional SEM image (inset: a plan-view SEM image of an ensemble of nanowires). (c) A cross-sectional TEM image. The nanowire density is approximately 7.8×10^9 cm^{-2}.

2.1 Epitaxial growth

After cleaning with acetone, isopropyl alcohol (IPA), and 20% hydrofluoric acid (HF), a diffusion barrier of tantalum nitride (TaN) about 20 nm thick was deposited on (100)-oriented Si substrates (resistivity $\rho = 10^{-1}$ Ω·cm) using atomic layer deposition (ALD) at 300 °C, followed by deposition of a layer of titanium (Ti) approximately 80 nm thick using an electron-beam physical vapor deposition (EBPVD) system. The Ta precursor was purged with argon (Ar) and hydrogen (H_2) plasma (flow rates of 200 and 50 sccm, respectively). The Ti/TaN/Si template was then outgassed in a plasma-assisted molecular beam epitaxy (PA-MBE) system load lock at 200 °C for one hour, followed by a second outgassing process in the system buffer chamber at 600 °C for two hours, to remove moisture and molecular adsorption in preparation for the subsequent nanowire growth. The n-type GaN seeds were initiated at a substrate temperature of 485 °C for ten minutes to reduce adatom desorption and enhance the probability of nucleation. The Ga beam equivalent pressure (BEP) was 6.2×10^{-8}

Torr, the Si effusion cell was kept at 1165 °C, and the high-brightness nitrogen (N) plasma was sustained using radio frequency (RF) power of 350 W at a 1-sccm flow rate. A second nucleation step at 585 °C lasting 20 minutes was employed to improve the GaN crystal quality. In total, n-type GaN layers averaging about 100 nm in thickness were grown, as verified via TEM imaging. The temperature was then elevated to 640 °C to grow a 50-nm-thick n-type AlGaN bottom barrier layer. We estimated the nominal Al atomic concentration from the ratio of the Al BEP compared to the Ga BEP. A nanowire active region was created by stacking ten repetitions of alternating $Al_xGa_{1-x}N$ quantum disks (QDisks, synthesized at Al and Ga BEPs of 0.75×10^{-8} Torr) and $Al_yGa_{1-y}N$ quantum barriers (QBs, synthesized at Al and Ga BEPs of 1.5×10^{-8} Torr), where $x < y$, grown at 640 °C, and with thicknesses of 3 nm and 4 nm, respectively. The approximately 50-nm-thick p-type top-contact AlGaN cap layer was then grown at 620 °C for 60 minutes at Al and Ga BEP values of 1.5×10^{-8} and 2×10^{-8} Torr, respectively, while the magnesium (Mg) cell temperature was kept at 440 °C with the same N plasma conditions. An additional highly doped layer of AlGaN (p^+-AlGaN) was grown atop the p-type AlGaN layer by increasing the Mg cell temperature to 450 °C and reducing the growth temperature to 580 °C, resulting in a p^+-AlGaN/p-AlGaN combined thickness of about 70 nm. We note that a narrower-bandgap p^+-GaN contact layer was not included in the design because such a layer may increase the UV optical absorption and decrease the efficiency of light extraction.[20,21]

2.2 Device fabrication

The UV-A nanowire-based LEDs were fabricated using standard UV contact lithography techniques. The grown nanowire samples were immersed in 20% HF to remove native oxide immediately before nickel (Ni)/gold (Au) (5 nm/5 nm) blanket-evaporation and one minute of rapid thermal processing (RTP). Further evaporation of Ni/Au (10 nm/400 nm) was carried out to define contact fingers and probe pads using photoresist and UV contact lithography, implemented via the metal-lift-off technique. Finally, the Si back-surface was etched away by around 200 nm using inductively coupled plasma reactive-ion etching (ICP-RIE; gas flow rates: SF_6 at 15 sccm; RF power of 50 W; ICP power of 500 W; and pressure of 10 mTorr) in preparation for forming the bottom n-type contact electrodes, Ti/Au (10 nm/150 nm).

3. DEVICE CHARACTERIZATION

3.1 Optical and electrical characterization

Figure 2(a) shows the electroluminescence spectra (χ_{EL}) for an ensemble of the UV-A quantum-confined nanowire-based LEDs at various temperatures from −50 °C to 100 °C. Figure 2(b) plots the evolution of the full spectral width at half maximum (FWHM) and the peak wavelength of emission (λ_{peak}) with increasing temperature. FWHM values varied between 22 nm and 26 nm, increasing gradually as the temperature rose from −50 °C to 100 °C, while λ_{peak} values varied between 321 nm and 326 nm, demonstrating strong and unprecedented operational stability across this wide range of operating temperatures.

Figure 3(a) shows the measured injection current density–applied forward voltage (J–V_F) curves for parylene-free and planarized LED samples between −50 °C and 100 °C, whereas Figure 3(b) displays semilogarithmic J–V_F curves at 100 °C. The evolution of the sub-turn-on voltage (V_{ON}) and onset current density (J_{ON}) across the same range of temperatures is shown in Figure 4(a) for both LEDs. V_{ON} values for the planarized LED decreased almost linearly from 9.28 V at −50 °C to 5.75 V at 100 °C as a result of bandgap shrinkage with increasing temperature, which is described by the Varshni equation:[22]

$$E_g(T) = E_g(0) - \frac{\alpha T^2}{T + \beta}, \tag{2}$$

where $E_g(0)$ is the band gap of an $Al_xGa_{1-x}N$ alloy at $T = 0$ K; α is an empirical constant (i.e., Varshni coefficient), and β is the Debye temperature.

Figure 5(a) shows the extracted ideality factor values, which were derived from the slopes of the semilogarithmic J–V_F curves at low V_F values, whereas Figure 5(b) depicts the extracted series resistance (R_s) values, which were extracted using linear fits of the linear-scale curves at high injection current levels.[3] The ideal p–n junction diode equation is[23]

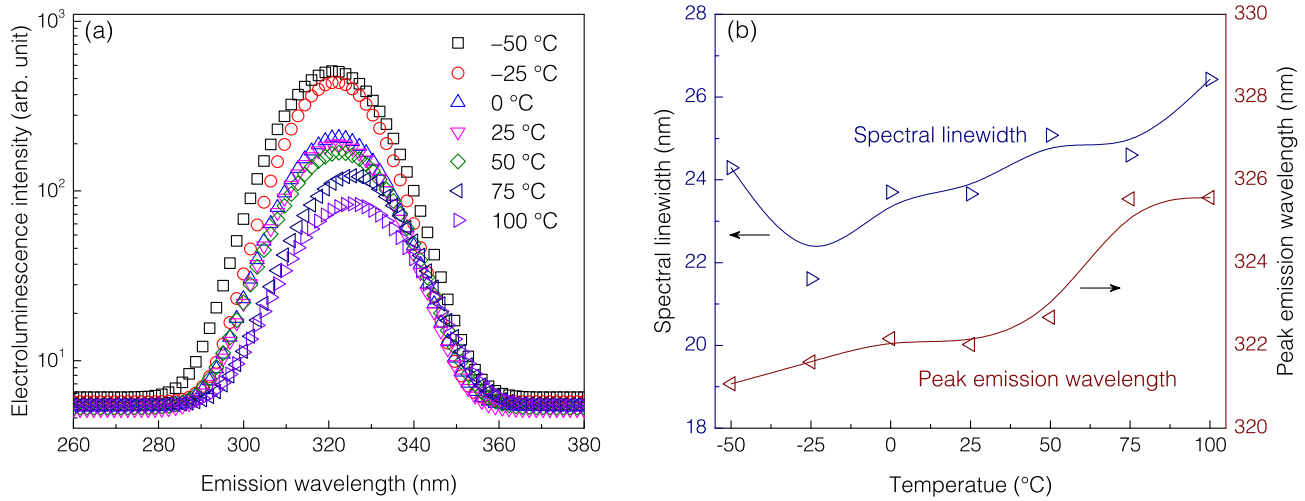

Figure 2. (a) Semilogarithmic scale χ_{EL} for parylene-free $\mathrm{Al}_x\mathrm{Ga}_{1-x}\mathrm{N}/\mathrm{Al}_y\mathrm{Ga}_{1-y}\mathrm{N}$ nanowire-based UV-A LED at various temperatures. (b) FWHM and λ_{peak} evolution with temperature.

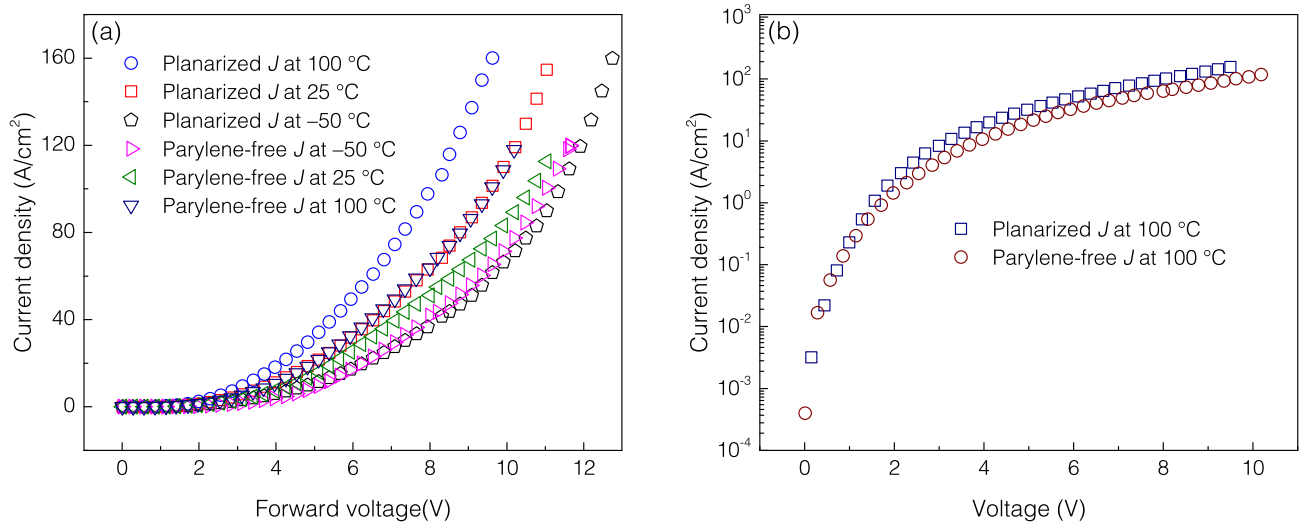

Figure 3. (a) Measured J–V_{F} curves for parylene-free and planarized $\mathrm{Al}_x\mathrm{Ga}_{1-x}\mathrm{N}/\mathrm{Al}_y\mathrm{Ga}_{1-y}\mathrm{N}$ nanowire-based UV-A LEDs at different temperatures prior to parylene-C deposition. (b) Semilogarithmic J–V_{F} curves at 100 °C for the parylene-free and planarized LEDs.

$$J = J_0(e^{\frac{qV_{\mathrm{F}}}{nkT}} - 1), \tag{3}$$

where I_0 is the saturation current density, q is the elementary charge, n is the ideality factor, and k is the Boltzmann constant. For $V_{\mathrm{F}} > \ell\frac{kT}{q}$, where ℓ is a multiplier designating a safe thermal voltage value yielding a simplified J–V_{F} relation (for $\ell = 3$, this yields about 60–100 mV within our operation temperature range), the exponential term dominates as $J \to J_0 e^{\frac{qV_{\mathrm{F}}}{nkT}}$ and equation (3) can be reduced to

$$J = J_0 e^{\frac{qV_{\mathrm{F}}}{nkT}}, \qquad \text{for } V_{\mathrm{F}} > \ell\frac{kT}{q}. \tag{4}$$

In an ideal p–n junction diode, $n = 1$ as the carrier recombination is determined by minority carriers through Shockley–Read–Hall (SRH) and band-to-band recombination processes.[24] We extracted n values from each J–V_{F}

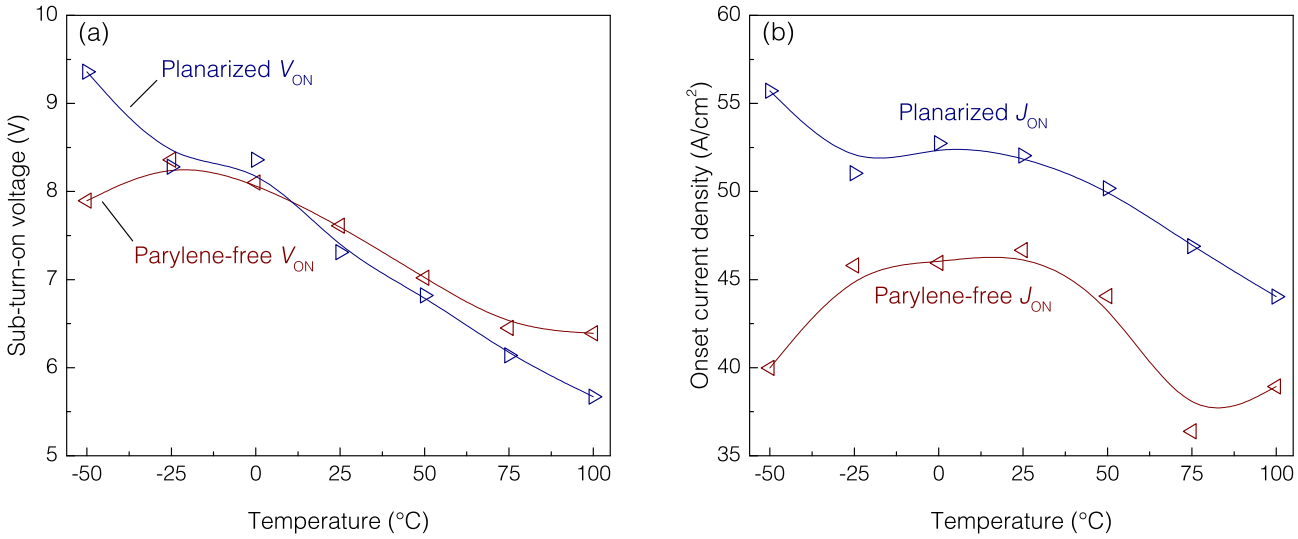

Figure 4. Evolution of (a) V_{ON} and (b) J_{ON} values with increasing temperature for parylene-free and planarized LEDs.

curve using linear fitting, where the slope (m_θ) is equal to $\frac{q}{nkT}$ at V_F values between 150 and 900 mV ($\ell > 5$ for $T \in [-50, 100]$) as follows:

$$\ln(J) = \ln(J_0) + \frac{q}{nkT} V_F, \tag{5}$$

exemplifying an ideal p–n junction diode J–V_F characteristic theory predicting a $V_F > 0$ semilogarithmic plot with a linear region slope of $\frac{q}{kT}$ and an extrapolated intercept of $\ln(J_0)$.[23]

As observed in Figure 5(a), n values for the planarized and parylene-free LEDs are generally close in value. The parylene-free LED sample exhibited an n value at 100 °C that was 18.17% higher than that of the planarized sample at the same temperature. The planarized LED sample showed a pronounced decreasing linear trendline as the temperature increased from −50 °C to 100 °C, while the trend curve for the parylene-free LED n values exhibited monotonic wave-like behavior, suggesting the activation of non-radiative recombination channels at temperatures higher than 0 °C induced by surface defect states, assuming that the non-radiative recombination centers are predominantly thermally inert at −50 °C.

3.2 Discussion

The planarized LED sample exhibited lower V_{ON} values above 0 °C. This behavior indicates the significant absence of interface charges resulting from silicide-induced interfacial reactions. Notably, we achieved a considerable increase in J up to 140 A/cm^2 at a $V_F = 11$ V at room temperature compared to our previous report, where we achieved injection current densities of up to 90 A/cm^2 at the same conditions.[18] Also, as can be seen in Figure 4(b), the planarized LED sample showed significantly enhanced J_{ON} values across the entire temperature range (11.50% worst-case enhancement at −25 °C and 25 °C and 39.30% best-case enhancement at −50 °C). The enhancement in J_{ON} at 100 °C was about 13.10%. We attribute this improvement in device performance to the mechanical scaffolding of contact layers and passivation of surface energy defect states provided by the parylene-C planarization layer, which presumably suppressed parasitic harmonics and dangling bonds, thereby decreasing the total harmonic distortion and diminishing Fermi level pinning, respectively, thus demonstrating enhanced electroluminescent cooling characteristics.[25–27] The wide depletion layer region caused by Fermi level pinning results in a reduction in the free electron density near the semiconductor nanowire surfaces, thereby increasing the non-radiative recombination in the active regions and adversely affecting its quantum efficiency.[3,28] As confirmation, we observed a maximum J value of about 100 A/cm^2 at $V_F = 11$ V at room temperature from the J–V_F measurements on the parylene-free LED sample (compared to 140 A/cm^2 in the planarized sample, as reported earlier). Parylene-C is known to significantly suppress UV emission below 280 nm.[29]

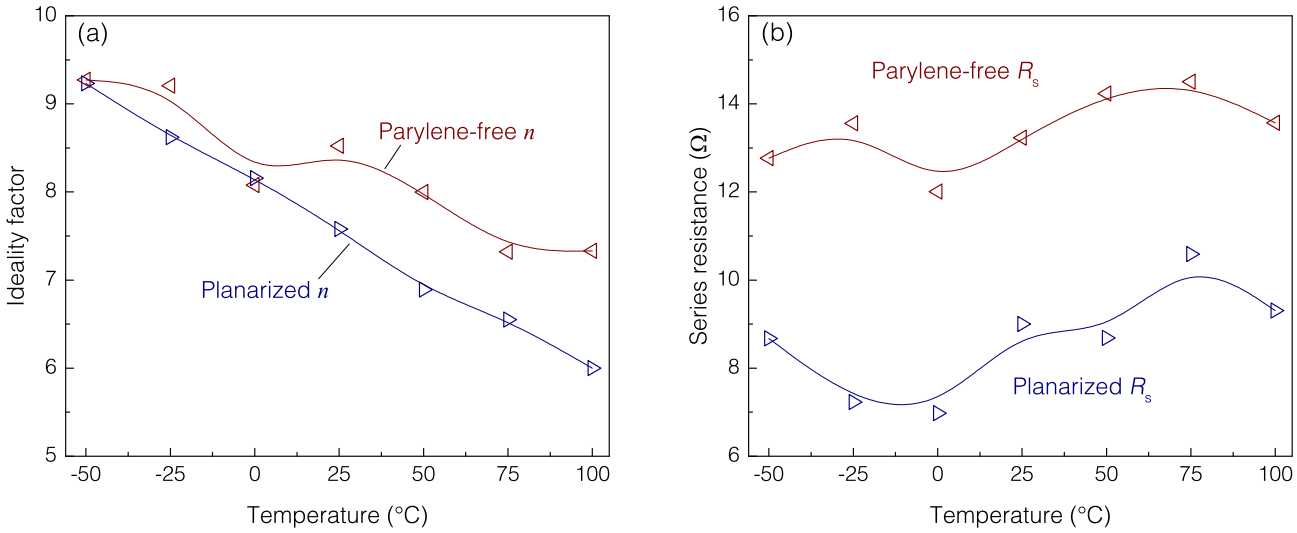

Figure 5. Evolution of (a) n and (b) R_s values with increasing temperature for parylene-free and planarized LEDs.

As can be seen in Figure 5(a), n values are relatively very high for the planarized and parylene-free LEDs, which we attribute to the high density of surface defect states exhibited by both devices. Nevertheless, the parylene-free LED exhibited more pronounced deviation from an ideal p–n junction diode behavior for $T > 25$ °C than did the planarized LED. The former exhibited n values that were 11.08%, 13.87%, 10.52%, and 18.17% higher than that of the planarized sample at 25, 50, 75, and 100 °C, respectively. We conjecture that the thermal energizing of surface defect states at temperatures higher than 0 °C resulted in these significant differences in n values because the planarized LED is less prone to surface defects, a fact that may be attributable to the effectiveness of the nanowire surface passivation provided by the parylene-C layer.[30] The R_s values for both LEDs as depicted in Figure 5(b) show that the planarized LED enjoys significantly lower R_s values across all operation temperatures, with a best-case reduction in R_s value of 46.68% at −25 °C and worst-case reduction of 27.00% at 75 °C. Using the ABC model, we previously confirmed that SRH recombination (A coefficient) dominates the carrier recombination processes at low J levels.[19] Therefore, non-radiative recombination processes affect the device performance at low injection current levels, while radiative recombination processes dominate at higher injection levels. Because R_s values were extracted from the LED J–V_F curves at high J values, the adverse effects of surface states (resembling non-radiative carrier recombination centers) are less pronounced. Lower R_s values of the planarized LED confirm the improved performance attributed to the parylene-C treatment of the sample. However, surface defect states cause less sharp turn-on characteristics because they attract carriers, preventing them from recombining radiatively. The various effects of surface defect states must be studied in more detail to establish plausible assumptions and verify our conjectures.

4. CONCLUDING REMARKS

In summary, we achieved enhanced performance of UV-A multiple-quantum-disk AlGaN-based nanowire LEDs on metal after parylene-C planarization, and we investigated the operational stability of the devices across a wide range of temperatures as would be experienced in harsh-environment operation, such as downhole photosensing. Our planarized LEDs showed a 1.4-times improvement in room-temperature injection current densities compared to the parylene-free LEDs. Planarized LED devices were shown to be highly stable across a wide range of operating temperatures and therefore suitable for operation in high temperatures and harsh environments. Furthermore, parylene-C planarized LEDs showed consistently higher onset current density values than parylene-free LEDs. Plans for future work include performing more temperature-dependent investigations to calculate internal and external quantum efficiencies of the device.

ACKNOWLEDGMENTS

The authors acknowledge the financial support of King Abdulaziz City for Science and Technology (KACST), grant no. KACST TIC R2-FP-008. This work was partially supported by King Abdullah University of Science and Technology (KAUST) baseline funding, BAS/1/1614-01-01, and MBE equipment funding, C/M-20000-12-001-77 and KCR/1/4055-01-01.

REFERENCES

[1] Sun, H., Wu, F., Park, Y. J., Al Tahtamouni, T. M., Liao, C.-H., Guo, W., Alfaraj, N., Li, K.-H., Anjum, D. H., Detchprohm, T., Dupuis, R. D., and Li, X., "Revealing microstructure and dislocation behavior in BAlN/AlGaN heterostructures," *Appl. Phys. Express* **11**(1), 011001 (2017).

[2] Sun, H., Wu, F., Al Tahtamouni, T. M., Alfaraj, N., Li, K.-H., Detchprohm, T., Dupuis, R. D., and Li, X., "Structural properties, crystal quality and growth modes of MOCVD-grown AlN with TMAl pretreatment of sapphire substrate," *J. Phys. D Appl. Phys.* **50**(39), 395101 (2017).

[3] Priante, D., Tangi, M., Min, J.-W., Alfaraj, N., Liang, J. W., Sun, H., Alhashim, H. H., Li, X., Albadri, A. M., Alyamani, A. Y., Ng, T. K., , and Ooi, B. S., "Enhanced electro-optic performance of surface-treated nanowires: origin and mechanism of nanoscale current injection for reliable ultraviolet light-emitting diodes," *Opt. Mater. Express* **9**(1), 203–215 (2019).

[4] Zhao, C., Alfaraj, N., Subedi, R. C., Liang, J. W., Alatawi, A. A., Alhamoud, A. A., Ebaid, M., Alias, M. S., Ng, T. K., and Ooi, B. S., "III-nitride nanowires on unconventional substrates: From materials to optoelectronic device applications," *Prog. Quantum Electron.* **61**, 1–31 (2018).

[5] Alfaraj, N., Hussain, A. M., Torres Sevilla, G. A., Ghoneim, M. T., Rojas, J. P., Aljedaani, A. B., and Hussain, M. M., "Functional integrity of flexible n-channel metal–oxide–semiconductor field-effect transistors on a reversibly bistable platform," *Appl. Phys. Lett.* **107**(17), 174101 (2015).

[6] Ghoneim, M. T., Fahad, H. M., Hussain, A. M., Rojas, J. P., Torres Sevilla, G. A., Alfaraj, N., Lizardo, E. B., and Hussain, M. M., "Enhanced cooling in mono-crystalline ultra-thin silicon by embedded micro-air channels," *AIP Adv.* **5**(12), 127115 (2015).

[7] Tangi, M., Min, J.-W., Priante, D., Subedi, R. C., Anjum, D. H., Prabaswara, A., Alfaraj, N., Liang, J. W., Shakfa, M. K., Ng, T. K., and Ooi, B. S., "Observation of piezotronic and piezo-phototronic effects in n-InGaN nanowires/Ti grown by molecular beam epitaxy," *Nano Energy* **54**, 264–271 (2018).

[8] Ghoneim, M. T., Alfaraj, N., Sevilla, G. A. T., and Hussain, M. M., "Ultra-high density out-of-plane strain sensor 3D architecture based on sub-20 nm PMOS FinFET," in [*IEEE 15th International Conference on Nanotechnology (IEEE-NANO)*], 1422–1425 (2015).

[9] Miller, R. A., So, H., Chiamori, H. C., Suria, A. J., Chapin, C. A., and Senesky, D. G., "A microfabricated sun sensor using GaN-on-sapphire ultraviolet photodetector arrays," *Rev. Sci. Instrum.* **87**(9), 095003 (2016).

[10] Alheadary, W. G., Park, K.-H., Alfaraj, N., Guo, Y., Stegenburgs, E., Ng, T. K., Ooi, B. S., and Alouini, M.-S., "Free-space optical channel characterization and experimental validation in a coastal environment," *Opt. Express* **26**(6), 6614–6628 (2018).

[11] May, B. J., Belz, M. R., Ahamed, A., Sarwar, A., Selcu, C. M., and Myers, R. C., "Nanoscale electronic conditioning for improvement of nanowire light-emitting-diode efficiency," *ACS Nano* **12**(4), 3551 (2018).

[12] Song, K., Mohseni, M., and Taghipour, F., "Application of ultraviolet light-emitting diodes (UV-LEDs) for water disinfection: A review," *Water Res.* **94**, 341 (2016).

[13] Mullins, O. C., "Method of distinguishing between crude oils." US Patent 5,266,800 (1993).

[14] Al-Jassim, N., Ansari, M. I., Harb, M., and Hong, P.-Y., "Removal of bacterial contaminants and antibiotic resistance genes by conventional wastewater treatment processes in Saudi Arabia: Is the treated wastewater safe to reuse for agricultural irrigation?," *Water Res.* **73**, 277 (2015).

[15] Ford, J. V., Blankinship, T., Kasperski, B. W., Waid, M. C., and Christian, S. M., "Multi-channel detector assembly for downhole spectroscopy." US Patent 8,735,803 (2014).

[16] Priante, D., Elafandy, R. T., Prabaswara, A., Janjua, B., Zhao, C., Alias, M. S., Tangi, M., Alaskar, Y., Albadri, A. M., Alyamani, A. Y., Ng, T. K., and Ooi, B. S., "Diode junction temperature in ultraviolet AlGaN quantum-disks-in-nanowires," *J. Appl. Phys.* **124**(1), 015702 (2018).

[17] Alfaraj, N., Muhammed, M. M., Li, K.-H., Janjua, B., Aljefri, R. A., Sun, H., Ng, T. K., Ooi, B. S., Roqan, I. S., and Li, X., "Thermodynamic photoinduced disorder in AlGaN nanowires," *AIP Adv.* **7**(12), 125113 (2017).

[18] Priante, D., Janjua, B., Prabaswara, A., Subedi, R. C., Elafandy, R. T., Lopatin, S., Anjum, D. H., Zhao, C., Ng, T. K., and Ooi, B. S., "Highly uniform ultraviolet-A quantum-confined AlGaN nanowire LEDs on metal/silicon with a TaN interlayer," *Opt. Mater. Express* **7**(12), 4214 (2017).

[19] Janjua, B., Priante, D., Prabaswara, A., Alanazi, L., Zhao, C., Alhamoud, A. A., Alias, M. S., Albadri, A. M., Alyamani, A. Y., Ng, T. K., and Ooi, B. S., "Ultraviolet-A LED based on quantum-disks-in-AlGaN-nanowires—Optimization and device reliability," *IEEE Photonics J.* **10**(2), 2200711 (2018).

[20] SaifAddin, B. K., Almogbel, A., Zollner, C. J., Foronda, H., Alyamani, A., Albadri, A., Iza, M., Nakamura, S., DenBaars, S. P., and Speck, J. S., "Fabrication technology for high light-extraction ultraviolet thin-film flip-chip (UV TFFC) LEDs grown on SiC," *Semicond. Sci. Technol.* **34**(3), 035007 (2019).

[21] SaifAddin, B., Zollner, C. J., Almogbel, A., Foronda, H., Wu, F., Albadri, A., Al Yamani, A., Iza, M., Nakamura, S., DenBaars, S. P., and Speck, J. S., "Developments in AlGaN and UV-C LEDs grown on SiC," in [*Light-Emitting Diodes: Materials, Devices, and Applications for Solid State Lighting XXII*], **10554**, 105541E, International Society for Optics and Photonics (2018).

[22] Varshni, Y. P., "Temperature dependence of the energy gap in semiconductors," *Physica* **34**(1), 149–154 (1967).

[23] Pierret, R. F., [*Semiconductor Device Fundamentals*], Addison-Wesley, Boston, 249–250 (1996).

[24] Hu, Z., Nomoto, K., Song, B., Zhu, M., Qi, M., Pan, M., Gao, X., Protasenko, V., Jena, D., and Xing, H. G., "Near unity ideality factor and Shockley-Read-Hall lifetime in GaN-on-GaN *p-n* diodes with avalanche breakdown," *Appl. Phys. Lett.* **107**(24), 243501 (2015).

[25] David, A., Hurni, C. A., Young, N. G., and Craven, M. D., "Electrical properties of III-nitride LEDs: Recombination-based injection model and theoretical limits to electrical efficiency and electroluminescent cooling," *Appl. Phys. Lett.* **109**(8), 083501 (2016).

[26] Alfaraj, N., Mitra, S., Wu, F., Ajia, I. A., Janjua, B., Prabaswara, A., Aljefri, R. A., Sun, H., Khee Ng, T., Ooi, B. S., Roqan, I. S., and Li, X., "Photoinduced entropy of InGaN/GaN p-i-n double-heterostructure nanowires," *Appl. Phys. Lett.* **110**(16), 161110 (2017).

[27] Kuritzky, L. Y., Weisbuch, C., and Speck, J. S., "Prospects for 100% wall-plug efficient III-nitride LEDs," *Opt. Express* **26**(13), 16600–16608 (2018).

[28] Calarco, R., Stoica, T., Brandt, O., and Geelhaar, L., "Surface-induced effects in GaN nanowires," *J. Mater. Res.* **26**(17), 2157–2168 (2011).

[29] Lu, B., Zheng, S., Quach, B. Q., and Tai, Y.-C., "A study of the autofluorescence of parylene materials for μTAS applications," *Lab Chip* **10**(14), 1826 (2010).

[30] Lee, B., Liu, X., Lee, K., Fan, D., Jung, B. J., and Forrest, S. R., "Surface passivation of InP using an organic thin film," *J. Cryst. Growth* **503**, 9–12 (2018).